Supporting information for

Two-Dimensional Flexible High Diffusive Spin Circuits

I. G. Serrano[1§], J. Panda[1§], Fernand Denoel[1§], Örjan Vallin[2], Dibya Phuyal[1], Olof Karis[1], and M. Venkata Kamalakar[1]*

[1]Department of Physics and Astronomy, Uppsala University, Box 516, SE-751 20, Uppsala, Sweden
[2]Department of Engineering Sciences, Uppsala University, Box 534, SE-751 21, Uppsala, Sweden

[§]authors contributed equally and are co-first authors.
*Email: venkata.mutta@physics.uu.se

1. CVD graphene transfer and Raman spectroscopy

A copper foil containing CVD graphene (from Graphenea) was attached to a heat release tape to ensure the mechanical stability necessary for spin coating of the polymethyl methacrylate (PMMA) resist layer. The copper from the Cu|graphene|PMMA stack was then etched out completely by a ferric chloride solution, followed by rinsing in dilute hydrochloric acid, and washing with deionized water. The PMMA layer containing graphene was transferred to a PEN substrate. Post-transfer, the substrate containing the film was dried, first by heating at 110 °C, and then placed in a vacuum chamber prior to further processing. As can be observed in Fig. S1.1, the PMMA edge in the middle of the frame is visible clearly. It is possible to distinguish the side of the substrate with PMMA from the clear side of the PEN without PMMA. The PMMA layer was dissolved in hot acetone, followed by rinsing with isopropanol. The substrate containing the CVD graphene was dried and heated at 110 °C, following which nanofabrication was performed.

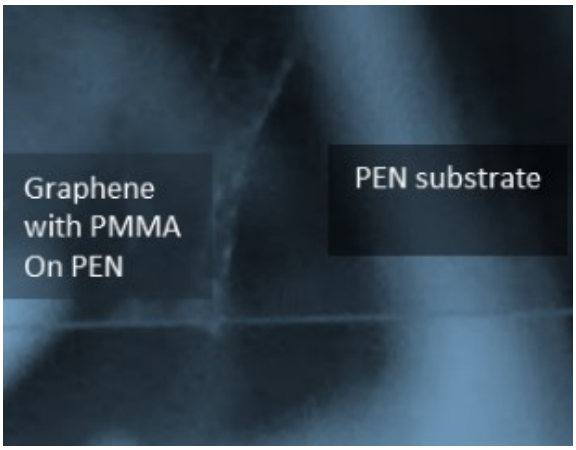

Fig. S1.1. A final dried layer of graphene|PMMA on PEN substrate.

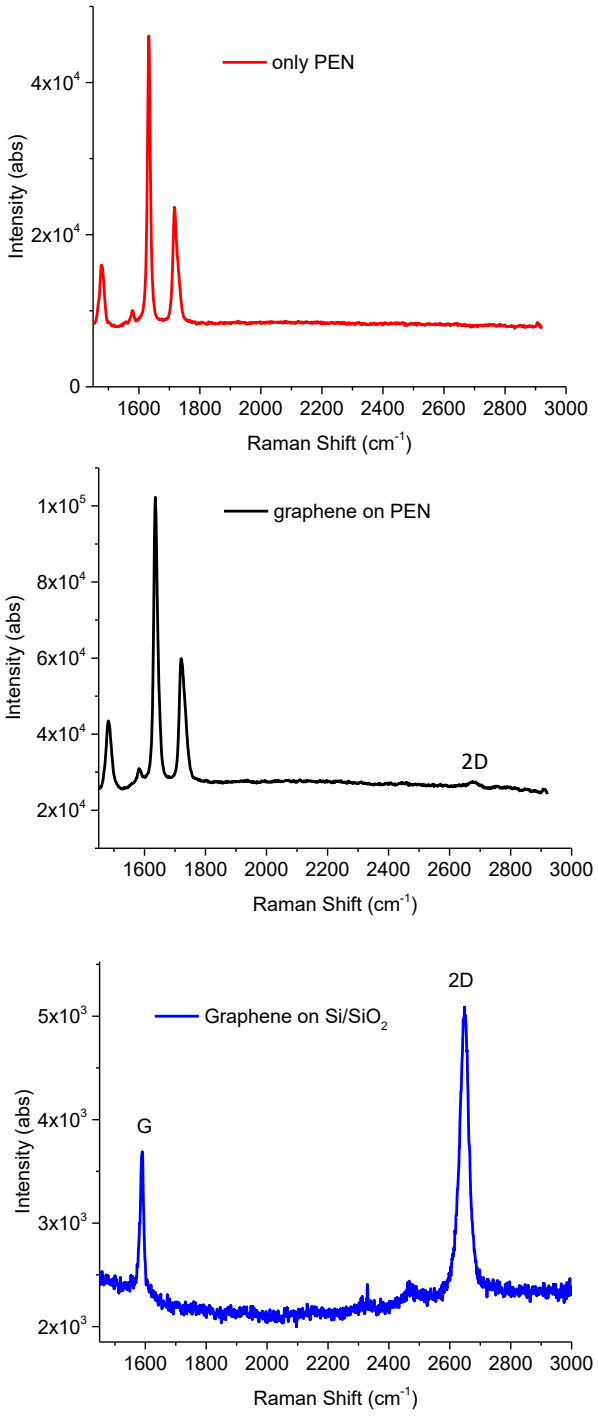

Fig. S1.2. Raman spectrum of PEN substrate, CVD graphene on PEN and Si/SiO_2 substrates.

In general, CVD graphene grown on the copper substrate is monolayer graphene due to the self-limiting growth process. It is difficult to characterize graphene over PEN using Raman spectroscopy due to the high background intensity (in Fig. S1.2). To assess the quality, we performed Raman spectroscopy of graphene over SiO_2, which showed an intensity ratio of 2D and G peak ~2 indicating single-layer graphene.

2. Optimum resistance of spin viable contacts

Fabricating electrodes with contact resistance ideal for spin injection is one of the prime challenges in realizing spin transport through graphene. Although it is possible to obtain low resistance contacts by directly depositing a ferromagnetic (FM) metal on graphene, such contacts are prone to contact-induced spin relaxation resulting in very weak or undetectable spin signals. The migration of FM atoms into the graphene lattice can also lead to spin relaxation, which makes it necessary to isolate the FM spin polarizer from the graphene layer. Conventionally, oxide barriers (TiO_2, MgO, Al_2O_3), and more recently, two-dimensional insulating crystals[1–3] have been employed to achieve efficient spin injection into graphene. Although tunneling-based electrical injection of spin-polarized electrons into graphene is efficient, such contacts possess significantly high resistance. While increasing the contact resistance can mitigate the problem of contact-induced spin relaxation, too high resistance values make the contacts unsuitable electrically, and enhance scattering and spin relaxation due to longer dwell times. Considering such factors, the dimensions and channel resistance of the non-magnetic (NM) component of a spin valve (FM-NM-FM structure with resistance R), the optimum range for efficient spin injection can be estimated using the Fert-Jeffrè model[4,5]. The model gives the value of calculated 2-terminal magnetoresistance $\Delta R/R$ (MR) as a function of the contact resistance of the FM-NM junction, revealing a range of contact resistance suitable for observing efficient spin transport. Fig. 5b in the main manuscript is based on this calculation[3–5].

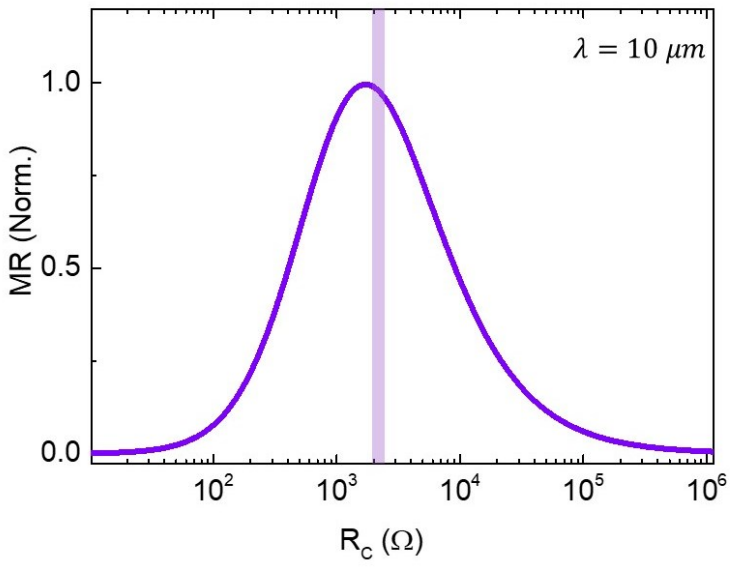

Fig. S2. **Calculated spin signal as a function of tunnel contact resistance**. Dependence of 2-terminal magnetoresistance (MR) on the contact interface resistance as calculated using the Fert-Jeffrè model[4,5] (calculated with device-1 electrical parameters). The shaded region indicates the contact resistances in device-1.

The ideal window of optimum contact resistance for graphene spin device-1 is shown in figure Fig. S2, where the variation of the two-terminal magnetoresistance of a graphene spin valve is plotted as a function of the contact resistance of the spin injection/detector electrodes. As shown in Fig. S2, by optimizing the titanium seed layer processing prior to depositing Co|Au, we were able to obtain the necessary contact resistance (measured by three-terminal measurements described in the main article) for spin signal observation. The obtained range of contact resistances in our device-1 is shown by the shaded region. Depending upon the variation in graphene sheet resistance, variation in the device to device electrical parameters have been observed (as seen in device-2). We confirmed the resilient magnetic nature of the contact electrodes by fabricating arrays of such nanowires of similar widths on the PEN substrate and performing in-situ bending magneto-optic Kerr microscopy.

3. Hall Effect: Carrier concentration and mobility

There are several methods for estimating the carrier mobility and concentration in graphene. One of the most common ways for graphene devices on Si/SiO_2 substrates is to measure the field effect mobility from the conductivity of a graphene channel recorded as a function of varying gate voltage. In Si/SiO_2 substrates, one can utilize a highly doped Si as the back gate electrode. The widely reported values of such field effect mobility are $\sim$ 2000 $cm^2V^{-1}s^{-1}$ for both exfoliated and CVD graphene on Si/SiO_2 substrates. In the case of flexible PEN substrate, there is no such possibility to apply a back gate due to the insulating nature of the entire substrate. While it is possible to fabricate a top gate on graphene by depositing an oxide layer such as titanium dioxide or aluminum oxide, this could dope graphene and alter its pristine electronic quality. To bypass such issues, we chose to perform Hall Effect experiments on several samples with varying square resistance from the same quality CVD graphene. In Fig. S3, we display the Hall voltage signal of a sample measured in a standard Hall configuration (shown in the inset of the figure). From these measurements, we obtain a carrier concentration $n = \frac{I\partial \boldsymbol{B}}{e\,|\partial V_H|} \sim 10^{12}\,cm^{-2}$ ($n \approx 0.9\text{-}2.04 \times 10^{12}\,cm^{-2}$) in Hall devices with R_{Sq} within the range of the electrical resistances of spin transport devices at room temperature, which leads to an estimated carrier mobility $\mu = \frac{1}{R_{Sq}\,n\,e} \sim (1\text{-}1.5) \times 10^4\ cm^2V^{-1}s^{-1}$ in low square resistance samples, assuming a mean to minimum carrier density. Although it is not possible to obtain the exact carrier concentration in the spin transport samples, the current approximation is a reasonable assumption[6] used for graphene samples on insulating substrates.

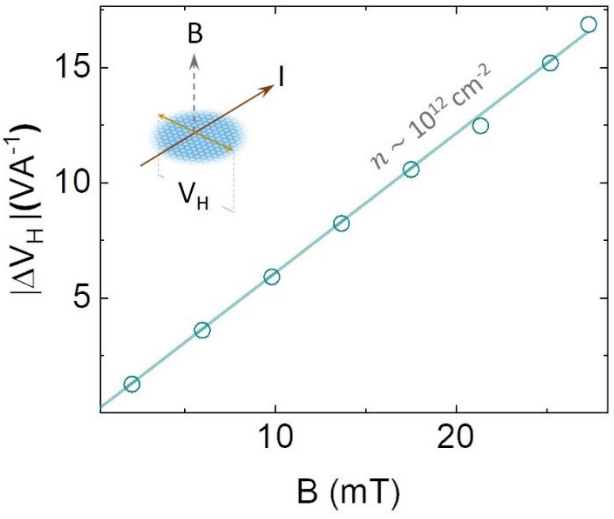

Fig. S3. **Hall effect measurement.** Hall voltage per unit current recorded as a function of magnetic field on a sample with a carrier concentration $n \sim 10^{12}\ cm^{-2}$. The inset shows the configuration of the Hall voltage measurement.

4. **Atomic force microscopy (AFM)**

The high-quality industrial-grade PEN substrates used for flexible electronic applications have surface roughness ~ 1.3 nm, a roughness that is much greater than that of Si/SiO_2 substrates. In Fig. S4a and S4b, an AFM scan of the topography of PEN substrate is shown (the thickness axis is not of the same scale when compared to the x and y-axes). A typical line scan of the surface (Fig. S4c) exhibits a roughness width ranging from 50-100 nm. A 1-2 nm peak distributed over 50-100 nm (roughness width) has a nearly flat nature with a negligible slope. In addition to that, an inspection of the intra-peak roughness (shown in Fig. S4d) reveals the root-mean-square roughness over the humps ~ Å, which indicates that the PEN substrate is significantly smoother than what one might expect from the overall roughness value.

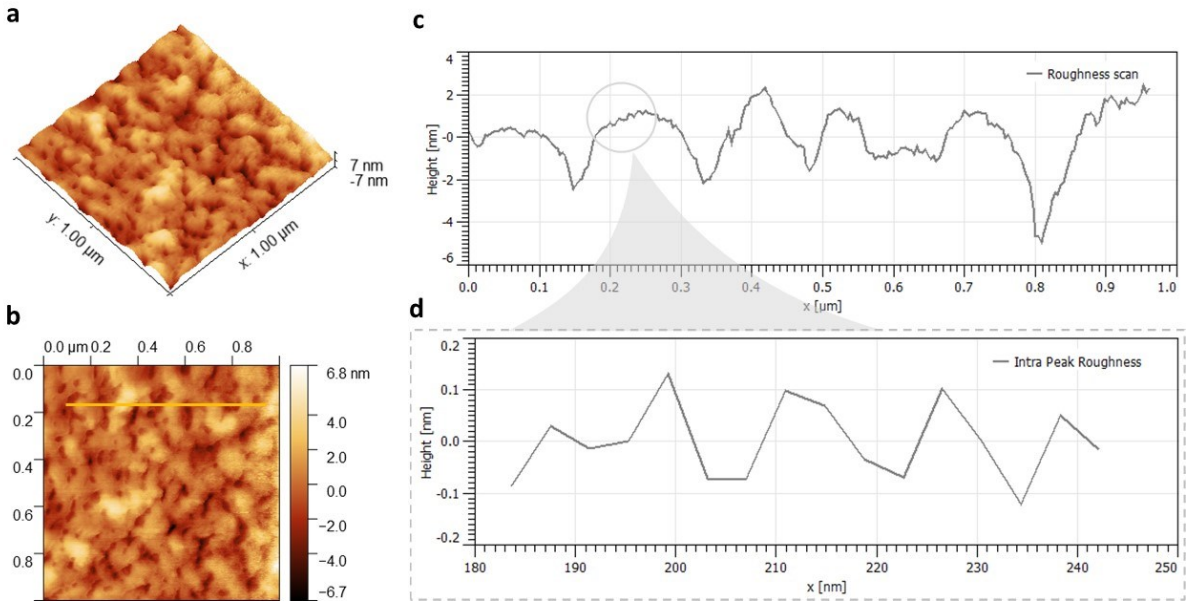

Fig. S4. **Atomic force microscopy of PEN substrate**. **a,** three-dimensional view of a 1 µm x 1 µm scan of the PEN surface. **b,** Atomic force microscope image with line scan. **c,** Line scan taken over the AFM image of the PEN substrate. **d**, A zoomed scan profile of the intra-peak roughness.

In Fig. S5a, we show atomic force microscopy of graphene over PEN that shows a similar roughness (R_q) as PEN suggesting that graphene conforms to the surface of PEN. The parameter Kurtosis K indicates the peak profile of a specific topography, with K > 3 for sharper peaks (as seen for graphene over Si/SiO_2 wafer, shown in Fig. S5b) and K < 3 (for graphene over PEN) for less sharp peaks.

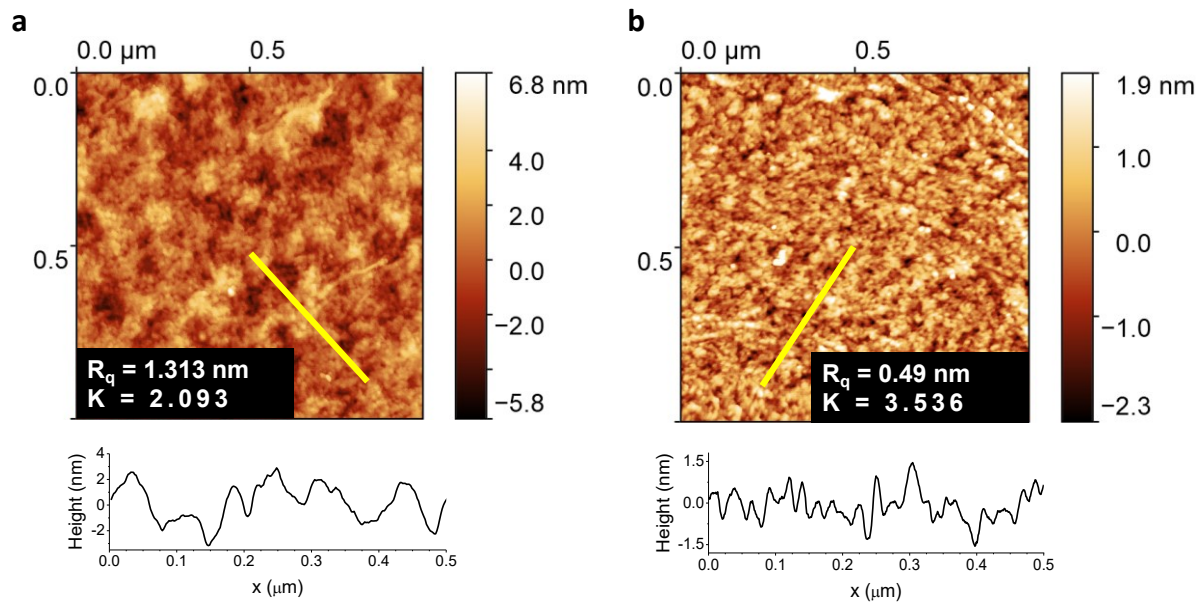

Fig. S5. **Atomic force microscopy**. **a,** graphene over PEN **b**, graphene over Si/SiO_2.

5. Characterization under bending condition

To understand the stability of FGSC under bending condition, we performed measurements under bending condition. In Fig. S6, we display the properties of a device measured in flat and bent conditions (radius ~ 5 mm).

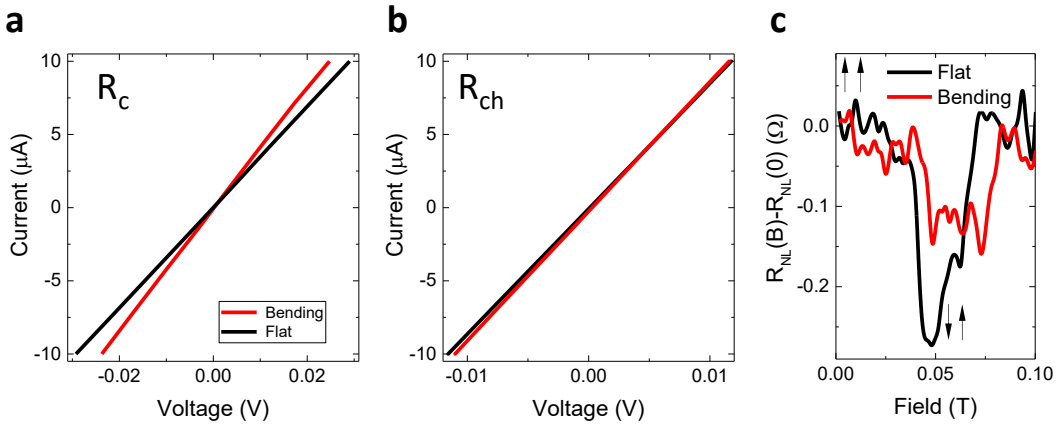

Fig. S6. **Stability test before and after bending. a,** Contact resistance **b**, Channel resistance. **c,** Spin valve switching obtained in a device in flat and bending conditions.

References

(1) Han, W.; Kawakami, R. K.; Gmitra, M.; Fabian, J. *Nat. Nanotechnol.* **2014**, *9* (10), 324–340.

(2) Friedman, A. L.; van 't Erve, O. M. J.; Li, C. H.; Robinson, J. T.; Jonker, B. T. *Nat. Commun.* **2014**, *5*, 3161.

(3) Kamalakar, M. V.; Dankert, A.; Bergsten, J.; Ive, T.; Dash, S. P. *Sci. Rep.* **2014**, *4*, 6146.

(4) Fert, A.; Jaffrès, H. *Phys. Rev. B* **2001**, *64* (18), 184420.

(5) Dlubak, B.; Martin, M.-B.; Deranlot, C.; Servet, B.; Xavier, S.; Mattana, R.; Sprinkle, M.; Berger, C.; De Heer, W. a.; Petroff, F.; Anane, A.; Seneor, P.; Fert, A. *Nat. Phys.* **2012**, *8* (7), 557–561.

(6) Maassen, T.; van den Berg, J. J.; Ijbema, N.; Fromm, F.; Seyller, T.; Yakimova, R.; van Wees, B. J. *Nano Lett.* **2012**, *12* (3), 1498–1502.